Sandpiles with Bistable Automata Rules: Towards a Minimal Model of Pedestal Formation and Structure

I. Gruzinov, P. H. Diamond, and M. N. Rosenbluth
University of California, San Diego, La Jolla, California 92093-0319
(Received 3 June 2002; published 5 December 2002)

A sandpile with two stable and two unstable ranges of slopes is presented as a minimal model for the study of H-mode pedestal formation and dynamics. Pedestals are observed to form and expand inward with increasing deposition. Transport bifurcation is not critical to pedestal formation, though the pedestal structure obtained with a second, hard stability boundary is qualitatively different from that found in standard sandpiles. Nonperiodic particle ejection events are observed, but do not initiate pedestal collapse. Pedestal formation alters the spectrum of transport avalanches.

DOI: 10.1103/PhysRevLett.89.255001 PACS numbers: 52.55.Dy

One of the most critical problems in fusion plasma physics is that of quantitatively understanding the structure of the H-mode [1] pedestal [2–4], a region of very steep profile gradients which forms at the plasma periphery after the $L \rightarrow H$ transition, when edge plasma turbulence is extinguished or drastically quenched. Since the pedestal temperature, determined by the product of the pedestal width and the pedestal slope, constitutes the "outer" boundary condition onto which the core profile must match, it is not surprising that the performance of tokamaks is very sensitive to the pedestal *width* [5]. This sensitivity is due in a large part to the facts that core ion temperature gradient turbulence is intrinsically stiff, thus tending to hover near marginal stability, and that the pedestal slope is constrained by relatively simple MHD stability considerations [6]. The major unknown is thus the pedestal width, which is determined by a complex interplay of turbulence and $L \rightarrow H$ transition dynamics, MHD stability limits, fueling profiles, and neoclassical transport processes. The usual approach to the pedestal width problem makes use of *ad hoc* considerations of parametric scaling in light of "typical" relevant lengths, such as the gyroradius or turbulence correlation length, neutral fueling length or poloidal gyroradius, etc.

In this paper, we report on studies of pedestal formation in a bistable sandpile — perhaps the simplest, most minimalistic model of this process. This simple model facilitates progress and allows insights not possible with more complete but vastly more complex models. However, we emphasize that our model is not yet capable of predictive quantitative modeling of pedestal phenomena. The model incorporates a toppling rule with a local gradient threshold and a second range of stability for gradients exceeding a second (larger) critical gradient. This second range loosely corresponds to the regime of diamagnetic electric field shear suppression of turbulence, characteristic of the H mode [7–9]. A second, hard stability boundary is set at a still larger slope, and loosely corresponds to the ultimate MHD stability limit on the pedestal gradient. Grain deposition is random and uniform. Obviously, grains should be thought of as units of density, so that the pedestal formation process studied here is somewhat like the pellet-induced H mode [10], which is triggered by internal particle deposition that increases the diamagnetic electric field shear.

A brief description of the model follows. The local slope Z_l defined as $Z_l = h_l - h_{l+1}$, where h_l is the lth cell's height, is stable when $Z_l < Z_{c1}$ or $Z_{c2} < Z_l < Z_{c3}$. If the local slope is in the first unstable range, i.e., $Z_{c1} \leq Z_l \leq Z_{c2}$, a fixed number of grains $D_z = 3$ is flipped from the unstable cell to the next one downhill, as in the standard sandpile models [11,12]. The rule for relaxation is different for the second instability, $Z_{c3} \leq Z_l$: we topple as many grains as needed to relax Z_l to a subcritical value $Z_{c1} - 1$. This flexibility in the size of a flip allows transport of all deposited sand to the edge without accumulation. The sandpile is $L = 100$ cells wide and constants Z_{c1}, Z_{c2}, and Z_{c3} are chosen to be 8, 20, and 30. As mentioned, the deposition is random and uniform. We start simulations from a flat sandpile. At each cycle, we add some sand at random cells, one grain per cell, and make a few iterations, defined by the deposition rate, N_f, which represents fueling or another driving mechanism (source of perturbation). (For example, if we are to simulate $N_f = 5/2$, we drop five grains and make two iterations during one cycle. Similarly, if $N_f = 3$, we deposit three grains and make one iteration per cycle, etc.) During an iteration, we check the slope for stability and update unstable cells *once*. It is important to note here that updating an unstable cell l means transporting a certain amount of sand to cell $l + 1$, which might make cells $l - 1$ or $l + 1$ unstable. Thus, at the end of a cycle some cells can be left unstable, and on the next cycle, new sand is added, etc. This algorithm accounts for a finite time of relaxation or mixing [13], and allows an interplay between deposited and transported fluxes. The sandpile can become supercritical, especially near the edge, can undergo transport bifurcation, and then can approach the profile stability limit. Indeed, the tendency of the sandpile slope to develop a supercritical gradient at the edge,

where the radial transport is also maximal, is well known even for uni stable models [14]. This is analogous to the tendency of the $L \rightarrow H$ transition to occur at the boundary, as pretransition profile steepening, which is necessary for a transport bifurcation, is most pronounced there. The sandpile takes approximately 100 000 iterations to reach its critical state. Then we run another 900 000 iterations in order to accumulate good statistics.

When deposition N_f exceeds the value that can be transported by a simple toppling D_z, the profile necessarily becomes steeper and steeper near the edge until the second, "hard" instability comes into play and a steady state is reached. The region of steepening of the profile is clearly bounded by a discontinuity in slope (Fig. 1). We call the region of steep profile a pedestal for two reasons. First, because it is intrinsically different from the edge steepening of the standard unistable sandpile models: in the latter case the slope near the edge is supercritical (i.e., unstable), while in our bistable model the *time-averaged* slope in the pedestal is *stable* with respect to the "MHD" instability which provides the transport in the pedestal, as will be shown below. Second, the pedestal region is bounded by a definite discontinuity in profile slope. An important observation here is that slope in the pedestal is independent of deposition (see Fig. 1).

The pedestal expands inward with increasing deposition. The steady-state widths for different deposition rates are shown in Fig. 2. For a fixed N_f, the width *fluctuates* about average value with no characteristic frequency. The width distribution is approximately Gaussian, with a variance slightly decreasing with width.

In simulations, we also found that the width and slope of the pedestal are essentially insensitive to the bifurcation threshold Z_{c2}. Thus, the steady-state pedestal is controlled by the hard MHD stability limit Z_{c3} *only*. Indeed, the pedestal is observed to form even when $Z_{c2} = Z_{c3}$, i.e., without suppression of first instability.

In Fig. 3, time sequences of slopes just before and immediately after the transition show the effect of the pedestal. The left panel is for the threshold deposition rate, $N_f = 3$. In this case, the steady-state sandpile arranges itself in the way that the last cell is always unstable and topples, thus maintaining a constant (3 grains per iteration) flux through the edge. Observe that transport bifurcation never occurs.

The right panel of Fig. 3 is for the deposition rate $N_f = 10/3$. Though the deposition is only slightly above the threshold, one sees the drastic changes in the dynamics of flux through the edge. It is not constant anymore, but is time intermittent with quiescent periods 2–20 iterations, and in rare cases as long as 60 iterations, with the average size of toppling being 12 grains (this toppling size is typical for the hard instability). The time-average flux through the edge is, of course, equal to the deposition rate. Usually, the avalanches started at the core are terminated at the pedestal shoulder, and transport through the edge is carried by second, MHD instability. In other words, the edge transport events usually do not destroy the pedestal. This is in distinct contrast to "giant" edge localized mode (ELM) phenomena. Pedestal destruction by a series of avalanches is a very rare event, and happens only after a long period of quiescence, during which the profile has been pushed to criticality. These large collapse events are *not* periodic. The precise relation between these edge ejections and the well-known phenomena of ELMs [15,16] is unclear, since some ELMs may involve global MHD instability processes [17] which are not included in our simple model here. We studied a statistics of quiescent periods between edge events. For deposition $N_f = 1$, the quiescent time τ distributed exponentially, a well-known fact for sandpiles; see Fig. 4, left panel. As deposition increases, the distribution changes its functional form. $N_f = 3$ is a special case: τ is always 0, as obvious from Fig. 3. For $N_f = 10/3$, the distribution of τ is well fitted by a Gaussian plus an exponential function $\propto e^{-\tau/6}$, as shown in Fig. 4, left panel. For larger N_f, the probability density function (PDF) of τ becomes a power law $\propto \tau^{-3.2}$ with an index essentially independent on N_f; see Fig. 4, right panel. Many systems, which are thought to exhibit intermittent behavior, show power law distribution of time periods between bursts. A relevant example can

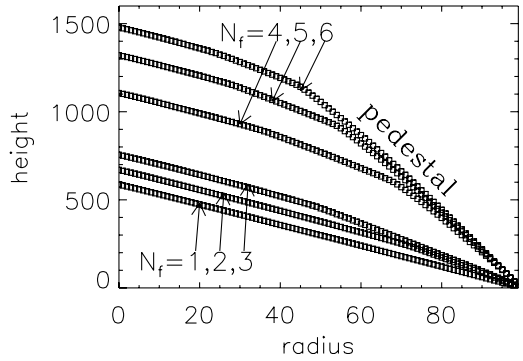

FIG. 1. Steady-state profiles for deposition rates $N_f = 1, 2, 3, 4, 5$, and 6. Observe the appearance of a steep gradient as N_f exceeds a critical value.

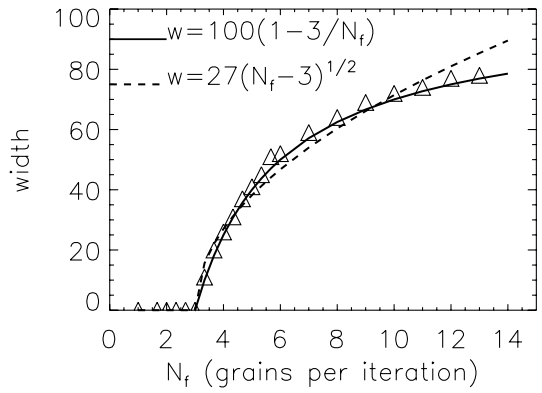

FIG. 2. Widths of the pedestal (triangles) in the simulations with different deposition rates N_f.

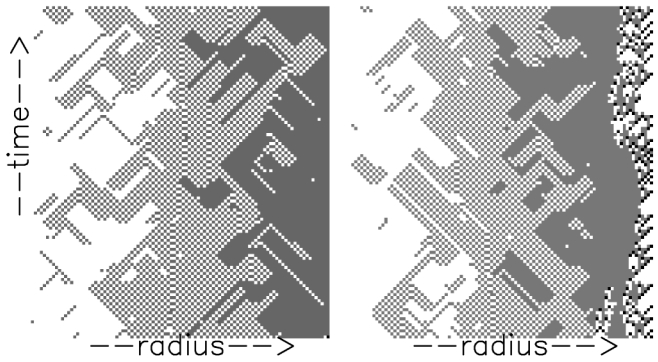

FIG. 3. The space-time pattern of the pile: white cells are *stable*, while gray and black cells are in first and in second *unstable* ranges of slopes, respectively. On the left: threshold deposition $N_f = 3$, and the pedestal is not formed. On the right: the deposition $N_f = 10/3$ exceeds the threshold and the pedestal appears. In this case, the transport through the edge is time intermittent.

be found in the study [18] of density fluctuations of magnetically confined plasma.

We have studied both the scaling of the mean flux with gradient and the spectrum of avalanches in the sandpile with the aim of elucidating how the formation of a pedestal affects each of these. N_f grains per iteration are distributed randomly through all cells and, eventually, have to be transported to the edge. Thus, one can readily calculate an *average* flux Γ_r through any cell at radius r and to relate it to an *average* local slope Z_r. Figure 5 is a family of parametric plots of $\Gamma(r)$ vs $Z(r)$ for N_f from 1 to 8. Γ as a function of Z is well defined and monotone for $Z \lesssim 10$ (i.e., in L mode and in the core region of H mode). The apparent slope steepening at $\Gamma \approx 1.5$ is a transition to a supercritical slope, characteristic of a standard sandpile [19]. Note that this is clearly distinct from the steepening associated with transport bifurcation. The slope jump $\Delta\Gamma/\Delta Z = 0$ at $\Gamma \approx 2.8$–3.0 is a pedestal shoulder. At the pedestal, where $Z_r > Z_{c2}$, $\Gamma(Z)$ branches into a family of curves, parametrized by N_f, in such a way that the slope at the edge stays constant $Z_{\text{edge}} \approx 23$. In other words, the *local* transport dynamics in the pedestal is strongly coupled to the *total* flux (which is equal to the deposition rate), and ultimately to the edge. Through this coupling, the slope in the pedestal is ultimately controlled by marginality to the hard (MHD) limit. This suggests an interesting departure from the conventional paradigm of local transport dynamics and emphasizes the edge effect on the pedestal. These could be thought of as sequences of falling dominos, for example. In L mode, the edge effect is not apparent, and the slope at the edge grows with deposition, as seen in Fig. 1.

Avalanches, namely, correlated topplings, that are space-correlated events in sandpiles with instantaneous mixing, should be defined as time-correlated events in our sandpile model. It is interesting to explore the effect of the pedestal on the avalanche size scaling. This constitutes a sandpile analog of ρ^* studies implemented on tokamaks. The main parameter used for statistical analysis of avalanche dynamics is the number of unstable cells at each time, $g(t)$. In our paradigm, this parameter characterizes the extent of turbulence activity. We count unstable cells separately in the core and in the pedestal to assess the affect of first and second instabilities. We find that PDF of flips in the core, and in the pedestal, and that of total number of flips are all Gaussian. The average number of flips per one grain added (that is, the average number of flips needed to transport one grain to the edge) is constant and independent of the deposition rate as long as the deposition rate is below threshold. This number starts to decrease as the pedestal grows and a larger fraction of flux is carried by second instability.

For deposition rates from 1 to 6, we calculate the power spectrum of flips, $P(\omega) = |g(\omega)|^2$. All spectra for $N_f \leq D_z$ are essentially indistinguishable: they show a flat low frequency region, followed by a short region with $P(\omega) \propto \omega^{-1}$, followed by a region with $P(\omega) \propto \omega^{-2.7}$, as seen in Fig. 6, left panel. Power spectra after transition are also indistinguishable from each other, though they differ substantially from spectra before the transition: a flat

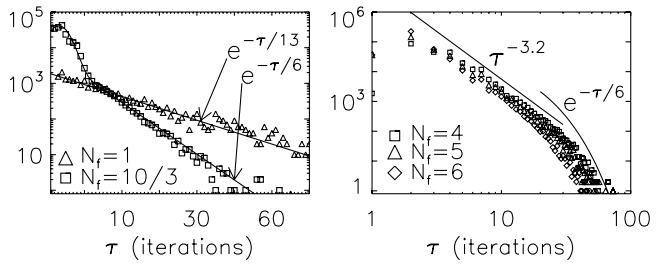

FIG. 4. Distributions of quiescent time between edge transport events. Left plot: for the marginal case of $N_f = 10/3$, when the pedestal just appeared; the fit for quiet time distribution is $e^{[10.5+(\tau-10/3)^2/12]} + e^{(9-\tau/6)}$, i.e., Gaussian + exponent. Right plot: when the pedestal is 30–50 cells wide, the main body of the distribution is a power law, and the tail is exponential.

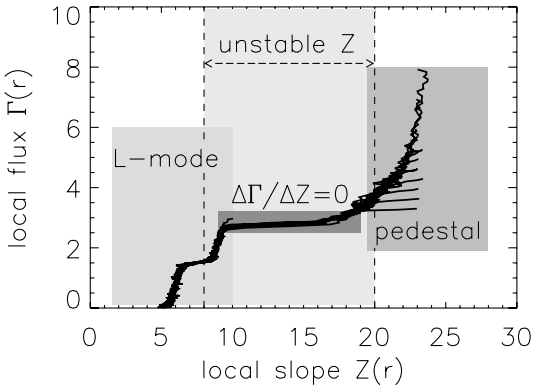

FIG. 5. Family of parametric plots of local flux $\Gamma(r)$ versus local slope $Z(r)$ for different depositions N_f from 1 to 8. The "transport" function $\Gamma(Z)$ is multivalued for $\Gamma > 3$.

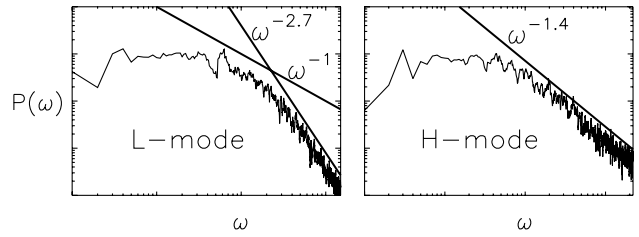

FIG. 6. Power spectra of flips for sandpiles in L mode ($N_f \leq 3$) and in H mode ($N_f > 3$). Note the change of power index from 2.7 to 1.4.

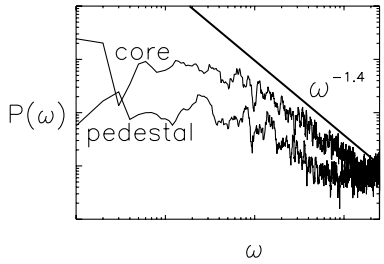

FIG. 7. Power spectra of flips in core and in pedestal regions for the case $N_f = 6$, when pedestal occupies $\approx 50\%$ of the pile. The power content of flips of the pedestal region is an order of magnitude smaller than that of the core, though the power index seems to be the same in both regions.

low frequency region is followed by $P(\omega) \propto \omega^{-1.4}$, as seen in Fig. 6, right panel, and the region $P(\omega) \propto \omega^{-1}$ seems to disappear.

As seen from Fig. 7, the dominant contribution to the power spectrum comes from flips in the core region; thus the effect of the pedestal is to truncate or obstruct long-range, low frequency events, which might connect the core to the edge. This observation also might explain the disappearance of the ω^{-1} range in the avalanche power spectrum—recall that ω^{-1} spectrum is a signature of long-range memory and self-similarity in avalanche dynamics [13]. It is interesting to observe that these trends are somewhat reminiscent of the "Bohm" scaling to the "gyro-Bohm" scaling change observed when comparing L-mode and H-mode plasmas [20,21]. Indeed, the sandpile studies suggest that the origin of this trend may be the fact that the pedestal prevents avalanches from "connecting" the core to the plasma boundary.

The simple bistable sandpile discussed here as a minimalistic model of confined plasma has yielded several interesting insights into pedestal structure and dynamics. Pedestal widths tend to fluctuate in time and expand inward with increasing deposition. The pedestal width is fit by the relation $w(N_f) = L(1 - N_{\rm crit}/N_f)$, where L is the pile size. The pedestal gradient is insensitive to the bistable transport law, and senses only the hard (MHD) stability boundary. Transport in the pedestal is determined by proximity to local MHD marginality. Moreover, the hard profile gradient limit operating in the pedestal forces a direct coupling of the *local* transport there to the deposition. The pedestal forms for uniform deposition. Thus, deposition scales and turbulence scales (here the latter is a cell size) are *not* intrinsic to the formation of pedestals. Moreover, even in the absence of global MHD events, the flux through the pedestal is intermittent, and consists of nonperiodically spaced bursts or ejections. The pedestal also shields the edge from core avalanches. Thus, pedestal formation alters the spectrum of avalanches by eliminating $1/\omega$ range and increasing the high-frequency content. Finally, this study also highlights the critical importance of an improved quantitative understanding of transport near MHD (i.e., peeling-ballooning) marginality [22] to a predictive model of pedestal structure and dynamics. This is apparent from the fact that many of the phenomena studied here stem from the presence of a second, hard stability boundary.

The authors thank J. Connor, A. Hubbard, R. Groebner, P. Gendrikh, and H. Wilson for useful discussions. The research was supported by DOE Grant No. DE-FG03-88ER53275.

[1] F. Wagner *et al.*, Phys. Rev. Lett. **53**, 1453 (1984).
[2] R. Groebner and T. Osborne, Phys. Plasmas **5**, 1800 (1998).
[3] R. Boivin *et al.*, in *Proceedings of the 26th EPS Conference on Controlled Fusion and Plasma Physics, Maastricht, 1999* (Max-Planck-Institut für Plasmaphysik, Munchen, 1999), Vol. 23J, p. 289.
[4] A. E. Hubbard, Plasma Phys. Controlled Fusion **42**, A15 (2000).
[5] R. Waltz (private communication).
[6] H. Wilson and J.W.Connor, in *Proceedings of the 24th EPS Conference on Controlled Fusion and Plasma Physics* (Max-Planck-Institut für Plasmaphysik, Munchen, 1997), Vol. 21A, p. 289.
[7] H. Biglari, P. Diamond, and P.W. Terry, Phys. Fluids B **2**, 1 (1990).
[8] F. I. Hinton, Phys. Fluids B **3**, 696 (1991).
[9] K. H. Burrell *et al.*, Phys. Plasmas **4**, 1499 (1997).
[10] P. Gohil *et al.*, Phys. Rev. Lett. **86**, 644 (2001).
[11] P. Bak, C. Tang, and K. Wiesenfeld, Phys. Rev. Lett. **59**, 381 (1987).
[12] L. Kadanoff *et al.*, Phys. Rev. A **39**, 6524 (1989).
[13] T. Hwa and M. Kardar, Phys. Rev. A **45**, 7002 (1992).
[14] D. E. Newman, B. A. Carreras, and P. H. Diamond, Phys. Plasmas **3**, 1858 (1996).
[15] H. Zohm, Plasma Phys. Controlled Fusion **38**, 105 (1996).
[16] J.W. Connor and H. R. Wilson, Plasma Phys. Controlled Fusion **42**, R1 (2000).
[17] P. B. Snyder *et al.*, Phys. Plasmas **9**, 2037 (2002).
[18] E. Spada *et al.*, Phys. Rev. Lett. **86**, 3032 (2001).
[19] M.V. Medvedev, P. H. Diamond, and B. A. Carreras, Phys. Plasmas **3**, 3745 (1996).
[20] C. Petty *et al.*, Phys. Rev. Lett. **74**, 1763 (1995).
[21] G. R. McKee *et al.*, Nucl. Fusion **41**, 1235 (2001).
[22] P. Diamond and T. Hahm, Phys. Plasmas **2**, 3640 (1995).